Tuning the microstructure and vortex pinning properties of YBCO-based superconducting nanocomposite films by controlling the target rotation speed

Tuning the microstructure and vortex pinning properties of YBCO based superconducting nanocomposite films by controlling the target rotation speed

Alok K. Jha[1]*, Kaname Matsumoto[1], Tomoya Horide[1], Shrikant Saini[2], Paolo Mele[2], Yutaka Yoshida[3], Satoshi Awaji[4]

[1] *Department of Materials Science and Engineering, Kyushu Institute of Technology, Tobata-ku, Kitakyushu 804-8550, Japan*

[2] *Institute for Sustainable Sciences and Development, Hiroshima University, Higashi-Hiroshima 739-8530, Japan*

[3] *Department of Energy Engineering and Science, Nagoya University, Chikusa-ku, Nagoya 464-8603, Japan*

[4] *Institute for Materials Research, Tohoku University, Aoba-ku, Sendai 980-8577, Japan*

* E-mail: akjha@post.matsc.kyutech.ac.jp

Abstract

We report the controlled incorporation of perovskite: $BaSnO_3$ (BSO) and double-perovskite: YBa_2NbO_6 (YBNO) nanocolumnar structures into $YBa_2Cu_3O_{7-\delta}$ (YBCO) film matrix by controlling the target rotation speed. Surface modified target approach has been employed to deposit YBCO+BSO and YBCO+YBNO nanocomposite films using laser ablation technique. The effect of target rotation speed on the microstructure and subsequently on the superconducting properties has been studied in detail. The density of BSO and YBNO nanocolumnar structures is found to depend on the target rotation speed, which subsequently affects the vortex pinning properties of the superconducting films in the absence and presence of applied magnetic fields. Three rotation speeds: 3 sec./rot., 2 sec./rot. and 1 sec./rot. have been attempted in this study. Compared to pure YBCO, the YBCO+BSO and YBCO+YBNO nanocomposite films exhibit superior in-field critical current density (J_C) and also

exhibit strong J_C peak for H//*c*-axis indicating strong *c*-axis pinning. The irreversibility line has also been found to improve significantly in the nanocomposite films. For both the target combinations (YBCO+BSO and YBCO+YBNO), the target rotation speed of 2 sec./rot. has been found to give the optimum superconducting properties.

1. Introduction

The introduction of artificial pinning centers (APCs) into $YBa_2Cu_3O_{7-\delta}$ (YBCO) superconducting film matrix has been recognized as being very effective for the immobilization of vortices leading to enhanced critical current density (J_C) and irreversibility field ($B_{irr.}$) of YBCO films [1]. In YBCO thin films, there is vortex pinning due to the presence of naturally occurring defects such as dislocations, grain boundaries, twin boundaries, oxygen vacancies, etc. However, majority of these defects are either not effective enough to suppress the thermal fluctuations or their densities are not high enough to maintain the necessary level of critical current density at large magnetic fields [2-4]. Various methodologies have been employed to introduce APCs into YBCO films which include irradiating the film with heavy ions [5], addition and/or substitution of rare-earth atoms [6, 7] or by adding the secondary phase nanoinclusions into the YBCO film matrix [8-17]. The incorporation of secondary phase nanoinclusions into YBCO superconducting film matrix for improving the vortex pinning properties has recently been extensively studied. The nanoinclusions of several non-perovskite, perovskite and double-perovskite materials such as Y_2O_3 [8], Y_2BaCuO_5 [9], $BaZrO_3$ [10, 11], $BaSnO_3$ [12, 13], $BaIrO_3$ [14], YBa_2NbO_6 [15, 16], YBa_2TaO_6 [17] have been demonstrated to enhance the vortex pinning properties of YBCO films deposited by pulsed laser deposition (PLD) technique.

In the PLD technique, the secondary phase nanoinclusions are usually introduced into the YBCO matrix by two methods: one by premixing the secondary phase material with YBCO and making a mixed target. Another approach is to use two different targets of YBCO and secondary phase material and switching them alternatively during deposition. The use of single premixed target offers desirable volume percentage of the secondary phase into the film matrix. However, it does not offer precise control on the size and distribution of the APCs throughout the thickness of the films formed during the deposition process. Another requirement of this process is that secondary phase material has to be non-reactive with YBCO in the sintering temperature range of 920-950 ℃ which is usually higher than the deposition temperature of the films (800-830 ℃).

A novel approach for introducing nanoscale secondary phase inclusions into YBCO film using PLD technique is to use surface modified target in which a thin sectored or rectangular shaped piece of secondary phase material is attached on the top of YBCO target using silver paste [18, 19]. In an earlier report, Mele *et al.* [20] have observed the formation of $BaZrO_3$ nanocolumns within the YBCO matrix for which they used YBCO+YSZ (yttria stabilized zircornia) surface modified target. There are several advantages of this approach over others, one of which is that the APCs can be continuously introduced into YBCO film matrix using single target in which YBCO portion and secondary phase material portion are physically separate. Another advantage of this approach is that the content of the secondary phase material can be finely tuned by changing the size of the sectored/rectangular shaped piece of secondary phase material while keeping the YBCO target as the same and/or by changing the rotation speed of the target during the ablation process.

The surface modified target approach is also interesting from the point of view of growth mechanism of different phases in a thin film. In the mixed target approach, there is continuous supply of adatoms or molecules of both the species (YBCO and other secondary phase) and the supersaturation of YBCO is higher than that of the secondary phase material (considering that the mixed target contains the secondary phase in less proportion than YBCO). However, in the surface modified target approach, the supply of the adatoms or molecules of different species takes place in an alternative and periodic manner and in this case the supersaturation of YBCO and the other secondary phase may be considered as the same. Despite these fundamental differences in these two approaches, the microstructure of the composite films reveals similar features: formation of nanocolumns of secondary phase within YBCO matrix. There must be some critical supersaturation state which separates the formation of nanocolumns from nanoparticles. The formation of nanoparticles of Y_2O_3 has been reported earlier also [8] but in that case, the formation of semi-coherent interfaces between the phases can be held responsible for such nanoparticle formation. Horide *et al.* [21] have reported the incorporation of gold nanorods with widely varying diameters into $GdBa_2Cu_3O_{7-\delta}$ (GdBCO) film. However, the driving force for the formation of gold nanorods within the GdBCO film matrix was not discussed. It may be quite interesting to investigate the critical supersaturation state, which separates the formation of nanocolumns from nanoparticles, between the species which are supposed to form coherent interfaces such as YBCO and other perovskite materials. The surface modified target approach can be a promising option in this direction.

In this paper, we present the effect of target rotation speed on the structural, microstructural and vortex pinning properties of YBCO thin films with varying

concentration of BSO and YBNO nanoscale inclusions. The concentration of secondary phase nanoinclusions is controlled by varying the target rotation speed during laser ablation process. The nanocomposite thin films showed superior J_C values along with remarkably improved irreversibility lines (*ILs*)

2. Experimental details

Thin films of YBCO and its nanocomposite with BSO and YBNO have been deposited on single crystal $SrTiO_3$ (STO) substrates using PLD technique (KrF excimer laser, λ = 248 nm). The schematic diagram of the deposition chamber is shown in figure 1 (a). The substrate temperature of 830 ℃ and O_2 partial pressure of 0.26 mbar was maintained during the deposition of the films. A repetition rate of 10 Hz was used while substrate to target distance was kept as 60 mm. For the deposition of pure YBCO thin film, a pristine YBCO target was ablated for 9,000 laser pulses whereas for YBCO+BSO and YBCO+YBNO nanocomposite films, the surface of the same YBCO target is modified as schematically illustrated in figure 1 (b). In the surface modified target approach, a sectored or rectangular piece of BSO or YBNO is attached to the top surface of YBCO target using silver paste. As the target is rotated, the BSO or YBNO portion is periodically ablated allowing the formation of BSO or YBNO nanocolumnar structures in the YBCO film matrix. Another schematics is shown in figure 2, which depicts that as the target rotation speed is changed, the ablation pattern from the surface modified target also changes resulting from the periodic ablation from YBCO and BSO or YBNO portions of the target. Three different rotation speeds with pulse frequency of 10 Hz have been tried in the present study: 1.0 sec./rot. (i.e., 60 rot./min.), 2.0 sec./rot. (i.e., 30 rot./min.) and 3.0 sec./rot. (i.e., 20 rot./min.). Thus 1.0 sec./rot. means the highest rotation speed while 3.0 sec./rot means the least rotation speed. It is expected that as the

rotation speed of the surface modified target is increased, the content of the secondary phase material (BSO or YBNO) will increase in the film matrix. The film deposited using YBCO+BSO surface modified target with target rotation speed of 1.0 sec./rot. is named as YBCO+BSO1.0, film deposited using YBCO+YBNO surface modified target with target rotation speed of 3.0 sec./rot. is named as YBCO+YBNO3.0 and so on. The thickness of as deposited thin films has been found to vary between 240-260 nm.

The microstructure and cross-sections of YBCO+BSO and YBCO+YBNO nanocomposite films have been studied using transmission electron microscopy (TEM). The electric transport measurement of the thin film samples has been carried out using Physical Property Measurement System (PPMS, Quantum Design) employing standard four-probe technique. Microbridges of 1 mm length and 60 μm width have been fabricated on the thin film samples using photolithography and wet-chemical etching technique. The resistivities of the thin film samples have been measured between 77 K and 300 K in zero applied magnetic field. The critical temperature (T_C) has been identified as the temperature where the resistivity (ρ) becomes 10^{-3} times the normal state resistivity (ρ_n) i.e., ($\rho/\rho_n = 10^{-3}$). A voltage criterion of 1 μvcm^{-1} is used to obtain the critical current values. Angular dependence of J_C of all the thin film samples was measured at 77 K and 1 T using the same voltage criterion.

3. Results and discussion

The strong *c*-axis orientation of pure YBCO, YBCO+BSO and YBCO+YBNO nanocomposite films has been ascertained from the X-ray diffraction measurement. The in-plane orientation has also been found to be reasonably good for all the thin film samples. The *c*-axis lattice parameter of the nanocomposite films, however, exhibited relative expansion compared to that of the pure YBCO film. Figure 3 shows the typical

cross-sectional TEM images of (a) YBCO+BSO3.0, (b) YBCO+BSO2.0, (c) YBCO+BSO1.0, (d) YBCO+YBNO3.0, (e) YBCO+YBNO2.0 and (f) YBCO+YBNO1.0 nanocomposite films. In all the TEM images, the formation of nanocolumnar structures can be observed clearly. In YBCO+BSO nanocomposite films it can be observed that the density of BSO nanocolumns is minimum in YBCO+BSO3.0, it increases in YBCO+BSO2.0 and is maximum in YBCO+BSO1.0 as per our anticipation. The diameter of the BSO nanocolumns is ~ 8-10 nm while the separation among them decreases with increasing target rotation speed. Similar trend can be observed in YBCO+YBNO nanocomposite films: the density of YBNO nanocolumnar structures being minimum in YBCO+YBNO3.0 increasing in YBCO+YBNO2.0 and maximum in YBCO+YBNO1.0. The diameter of YBNO nanocolumns is around ~ 6-8 nm and the separation decreasing with increasing target rotation speed. It can be seen that some of the YBNO nanocolumns are slightly tilted with respect to the *c*-axis of the films. The density of defects in samples deposited using varying target rotation speed can be approximately estimated from the TEM images (figure 3) by extrapolating the linear density into the areal density. Such an estimation leads us to obtain the defect density of 7.7×10^{10} cm^{-2}, 1.8×10^{11} cm^{-2} and 3.7×10^{11} cm^{-2} for the target rotation speeds of 3.0 sec./rot., 2.0 sec./rot. and 1.0 sec./rot. respectively. However, such an estimation has the possibility of some errors as the density of defects may vary along different directions. In both YBCO+BSO and YBCO+YBNO series, it can be concluded that the density of the APCs can be systematically varied by controlling the target rotation speed.

Figure 4 (a) shows the variation of the superconducting transition temperature (T_C) with target rotation speed for YBCO+BSO and YBCO+YBNO nanocomposite films. The T_C

for pure YBCO film is 89.8 K. The T_C values for YBCO+BSO1.0, YBCO+BSO2.0 and YBCO+BSO3.0 are 87.4 K, 87.7 K and 89.1 K respectively and the T_C values for YBCO+YBNO1.0, YBCO+YBNO2.0 and YBCO+YBNO3.0 are 87.7 K, 89.0 K and 88.8 K respectively. It is apparent from these values that the T_C of the YBCO+BSO and YBCO+YBNO nanocomposite films decreases as the target rotation speed is increased and it is reasonable to presume that the volume fraction of the secondary phase is increasing as the target rotation speed is increased. The increasing volume fraction of the secondary phase into YBCO film matrix may lead to substitution or strain resulting in the suppression of the T_C values. Apart from suppressed T_C values, the nanocomposite films also exhibit broader superconducting transition. The δT_C value for YBCO film is 1.2 K while for the YBCO+BSO and YBCO+YBNO nanocomposite films it varies from 1.9 K to 3.4 K. Figure 1 (b) shows the variation of δT_C with target rotation speed for YBCO+BSO and YBCO+YBNO nanocomposite films. The T_C and δT_C values for all the studied samples have been listed in table 1.

An extensive investigation of the superconducting properties will demonstrate the advantages of using the surface modified target approach and tuning the critical current properties by controlling the target rotation speed. Figure 5 shows the variation of J_C and pinning force density (F_p) with applied magnetic field for YBCO, YBCO+BSO and YBCO+YBNO nanocomposite films. In figure 5 (a), the variation of J_C with applied magnetic field for YBCO+BSO nanocomposite films at 77 K is shown. It can be seen that the J_C values for YBCO+BSO nanocomposite films are enhanced significantly as compared to that for pure YBCO film and this enhancement is more prominent at higher applied magnetic fields. It can be concluded that the BSO nanocolumnar structures are effective enough to improve the flux pinning properties of YBCO films. Figure 5 (b)

shows the variation of J_C with applied magnetic field for YBCO+YBNO nanocomposite films in comparison with that of pure YBCO film at 77 K. In the lower magnetic field regime (< 1 T), YBCO+YBNO1.0 and YBCO+YBNO3.0 films have J_C values lower than that for pure YBCO film, but at higher applied magnetic fields their J_C values exceed the J_C values of pure YBCO film. In contrast, the YBCO+YBNO2.0 nanocomposite film has J_C values significantly higher than that of the pure YBCO film over the entire investigated range of applied magnetic field. The J_C values at self-field and an applied magnetic field of 1 T at 77 K for all the thin film samples have been listed in table 1 for comparative analysis.

From the variation of J_C with B, power law dependence of J_C on B can be observed as per the equation ($J_C \propto B^{-\alpha}$) in the intermediate field regime (0.1-1.0 T) and the value of the exponent α has been obtained from the above relation. At 77 K, the value of α for YBCO thin film is 0.57 whereas, for YBCO+BSO and YBCO+YBNO nanocomposite films, its value was found to vary between 0.24 to 0.44. This means that the rate of decrease of J_C with magnetic field is smaller for YBCO+BSO and YBCO+YBNO nanocomposite thin films than that for YBCO thin film. There are several reports [22, 23] which have shown that BZO nanoparticles align themselves in the form of nanorods which act as extended defects effective for artificial pinning. In the present case also, self-assembled nanorods of BSO and YBNO have been observed in the cross-sectional TEM images which are supposed to be acting as effective artificial pinning centers.

In figures 5 (c) and 5 (d), the variation of F_p as a function of applied magnetic field for YBCO+BSO and YBCO+YBNO nanocomposite films at 77 K has been shown. At 77 K, the $F_{p\text{max.}}$ value for pure YBCO is 2.54 GNm^{-3} whereas it increases to 8.04, 10.57 and 4.55 GNm^{-3} for YBCO+BSO3.0, YBCO+BSO2.0 and YBCO+BSO1.0 films

respectively. Apart from $F_{p\max.}$ values increasing significantly, the applied magnetic field at which $F_{p\max.}$ occurs is shifted towards higher values in the YBCO+BSO nanocomposite films which means that pinning is more effective at higher applied magnetic field. On the other hand, the $F_{p\max.}$ values for YBCO+YBNO3.0, YBCO+YBNO2.0 and YBCO+YBNO1.0 films are 3.54, 7.01 and 3.89 GNm^{-3} respectively. These values are greater than the $F_{p\max.}$ value for YBCO film, but the applied magnetic field at which $F_{p\max.}$ occurs remains the same as for pure YBCO film. Moreover, the $F_{p\max.}$ values for YBCO+BSO nanocomposite films are better than the $F_{p\max.}$ values for YBCO+YBNO nanocomposite film deposited using same target rotation speeds.

In figure 6, the variation of J_C and F_p with applied magnetic field for YBCO+BSO and YBCO+YBNO nanocomposite films measured at 65 K has been presented. From these figures, it can be observed that the target rotation speed of 2.0 sec./rot. gives the optimum J_C and F_p values for both YBCO+BSO and YBCO+YBNO combinations. Furthermore, the J_C-B characteristics of YBCO+BSO films is found to be superior to YBCO+YBNO films at higher applied magnetic field which is reflected again in the higher $F_{pmax.}$ values of YBCO+BSO nanocomposite films. For comparison, the J_C and $F_{pmax.}$ values of these nanocomposite films obtained at 65 K have been summarized in table 1.

Figure 7 shows the variation of self-field J_C and $F_{pmax.}$ with target rotation speed for YBCO+BSO and YBCO+YBNO nanocomposite films at 77 K and 65 K. It can be seen that YBCO+YBNO nanocomposite films have higher self-field J_C values compared with YBCO+BSO nanocomposite films. However, the $F_{pmax.}$ values of YBCO+BSO nanocomposite films are substantially higher than that for YBCO+YBNO films. It

eventually means that the in-field performances of the YBCO+BSO films are superior to YBCO+YBNO films. If we look at the TEM images of these nanocomposite films, we observe some differences between the microstructures of YBCO+BSO and YBCO+YBNO nanocomposite films: one, the diameter of the BSO nanocolumns are larger than that of the YBNO nanocolumns and two, the density of the planar defects is higher in YBCO+BSO films than in YBCO+YBNO films. Also, the BSO nanocolumns are straight along the *c*-axis while the YBNO nanocolumns are slightly tilted with respect to the *c*-axis. The effect of columnar defects in YBCO films for improving the vortex pinning properties has been well established. Furthermore, the straightness of the secondary phase nanocolumnar structures throughout the thickness of the superconducting films and their diameter are important parameters which influence the pinning characteristics of YBCO films. In an earlier report, Nelson and Vinokur have expressed pinning energy per unit length near the columnar defects, based on the solution of London and Ginzburg-Landau equations, which is as follows [24]:

$$u_0 = \frac{1}{2}\varepsilon_0 \ln\left(1 + \left(\frac{C_0}{\sqrt{2}\xi_{ab}}\right)^2\right) \quad (1)$$

where, $\varepsilon_0 = (\Phi_0/4\pi\lambda_{ab})^2$, λ_{ab} and ξ_{ab} being the London penetration depth and the coherence length respectively in the *ab* plane, Φ_0 is the flux quantum and C_0 is the radius of the columnar defect. According to the given equation, pinning energy of the nanocolumnar structures is directly proportional to its radius (or diameter) and this has been demonstrated later by Mele *et al.* [25]. Thus our assumption for larger diameter of BSO nanocolumnar structures being responsible for higher pinning force density of the YBCO films is reasonable.

Further, looking at all the parts of figures 5 and 6, it can be observed that the target rotation speed of 2 sec./rot. gives the optimum critical current properties in both

YBCO+BSO and YBCO+YBNO nanocomposite films. In a previous report, Mele *et al.* [12], have shown that YBCO+BSO (4%) film (prepared using a mixed target) gave the optimum $F_{pmax.}$ value. However, as the concentration of BSO increases to 5% and 6% or decreases to less than 3%, the $F_{pmax.}$ values decrease substantially in their case also. Considering the frequency of laser ablation (10 Hz) and the target rotation speed, it can be roughly estimated that 1 rot./sec., 2 rot./sec. and 3 rot./sec. provide ~ 10%, ~5% and ~3% incorporation of secondary phases (BSO or YBNO) into YBCO matrix. However, this estimation may have little inaccuracy. It can be speculated that the BSO content in YBCO+BSO2.0 film is ~ 5% and if the target rotation speed around 2 rot./sec. is finely tuned, even better critical current performance may be realized.

Figures 8 (a) and (b) show the angular dependence of J_C for YBCO+BSO and YBCO+YBNO nanocomposite films respectively measured at 77 K and 1 T. The improved angular dependent J_C behavior can be clearly observed in YBCO+BSO nanocomposite films where strong improvement in the *c*-axis correlated pinning has been resulted from continuous BSO nanocolumnar structures. However, for YBCO+BSO1.0 film, even as the *c*-axis peak is enhanced significantly, *a*-*b* peak is suppressed somewhat presumably because of high density of continuous BSO nanorods which may prevent the intrinsic layer pinning [26]. In YBCO+BSO2.0 film, the enhancement in the J_C value along *c*-axis is 2-fold and it has exhibited the best $F_{pmax.}$ value among all the studied combinations. Overall, the YBCO+BSO nanocomposite films show reduced anisotropy as compared to the pure YBCO film. In the case of YBCO+YBNO nanocomposite films also, the anisotropy is reduced. Moreover, YBCO+YBNO2.0 nanocomposite film show strong enhancement in the J_C values not only along the *c*-axis but over the entire measured angular range. There is almost 3-fold

enhancement of J_C value along the *c*-axis while along the *a*-*b* plane 2-fold enhancement is observed.

Figure 9 shows the variation of irreversibility fields (above which loss-less transport of current ceases) with absolute temperature T and reduced temperature (T/T_C) for YBCO+BSO and YBCO+YBNO films in comparison with that of pure YBCO film. The $B_{irr.}$ for pure YBCO at 77 K has been estimated to be 8.8 T whereas at the same temperature, it increases up to 13.4 T in the case of YBCO+BSO2.0 film as determined from the extrapolation of the straight line portions of the irreversibility lines (*ILs*). The $B_{irr.}$ values for YBCO+BSO1.0 and YBCO+BSO3.0 has been estimated to be 10.0 T and 12.2 T respectively. There is a pronounced up-shift of the *ILs* and it becomes more prominent when $B_{irr.}$ is plotted against reduced temperature (T/T_C) which eliminates the effect of transition temperature. In the case of YBCO+YBNO nanocomposite films, the maximum $B_{irr.}$ at 77 K is 9.9 T which has been obtained for YBCO+YBNO2.0 film. For YBCO+YBNO1.0 and YBCO+YBNO3.0 films, the $B_{irr.}$ values are 7.9 T and 9.2 T respectively. In this case, the upward shift of the *ILs* is not as significant as in the case of YBCO+BSO films. In another report by Figueras *et al.* [27], the upper limit for effective pinning by linear/columnar defects has been estimated. The upper limit is designated by the characteristic field (B_L) above which the line tension of the vortices becomes negligible leading to strong dissipation. This characteristic field B_L is given by

$$B_L(t) = B_{C2}(t)\left[1 - \frac{g}{A}t(1-t)^{-0.5}\right] \quad (2)$$

where $B_{C2} = \frac{\Phi_0}{2\pi\xi^2}$ is the upper critical field, $\xi = 0.74\,\xi_0(1-t)^{-0.5}$, g = 0.09-0.12, A is a geometrical factor of the order of unity, and t is the reduced temperature (T/T_C). The parameter g is determined by parameters such as the critical temperature T_C and London

penetration depth. In figure 9 ((c) and (d)), B_L is drawn using $g/A = 0.10$ and this agrees well with the $B_{irr.}$ plots of the YBCO+BSO nanocomposite films. However, for YBCO+YBNO nanocomposite films, there is a slight deviation of the *ILs* from B_L below the matching field. In an earlier report by Horide *et al.* [28], the difference in the *ILs* has been discussed. It is described that the upward shift in the *ILs* is principally because of the morphology of the APCs and it is simply not related to the volume fraction of the secondary phase inclusions acting as APCs. More precisely, it is suggested that the continuous elongation of the nanocolumnar structure throughout the thickness of the film is very effective in improving the vortex pinning properties resulting in the upward shift of the *ILs*. Looking back at the TEM images, it can be seen that in the case of YBCO+YBNO nanocomposite films the continuity of the nanocolumns is disrupted in some portions and some of the nanocolumns are tilted slightly with respect to the *c*-axis of the films. In contrast, in the case of YBCO+BSO nanocomposite films, the continuation of the BSO nanocolumns is much better and there is minimal tilting of the nanocolumns with respect to the *c*-axis of the films. It can be concluded that continuous elongation of the BSO nanocolumnar structures is very useful for effective vortex pinning and BSO nanocolumns are more effective than the YBNO nanocolumns.

The analysis of the results presented in this paper indicates that the surface modified target is a promising method which can provide the controlled introduction of the APCs into YBCO film matrix by selection of the secondary phase material for surface modification and controlling the target rotation speed. It would be further interesting to fine tune the parameters for further improvement in the vortex pinning properties and also understand the growth mechanism of different phases by investigating and

controlling the supersaturation of the respective phases by adopting the surface modified target approach.

Conclusions

The controlled introduction of BSO and YBNO nanocolumnar structures into YBCO film matrix by controlling the target rotation speed has been demonstrated. In both YBCO+BSO and YBCO+YBNO nanocomposite films, the critical current properties have been improved and a significant upper-shift in the irreversibility lines has been observed. The YBCO+BSO films showed better J_C-B characteristics at higher applied magnetic fields and larger shift in the irreversibility lines which has been attributed to the continuous BSO nanocolumns having larger diameter. For both the combinations, the target rotation speed of 2.0 sec./rot. exhibited the best results which can be further improved by fine-tuning the rotation speed around 2.0 sec./rot.

Acknowledgement

This work was supported by KAKENHI, Grant-in-Aid for Science Research (S), Grant Number 23226014.

References:

[1] Matsumoto K and Mele P 2010 *Supercond. Sci. Technol.* **23** 014001

[2] Dam B, Huijbregtse J M, Klaassen F C, Van der Geest R C F, Doornbos G, Rector J H, Testa A M, Freisem S, Martinez J C, Stauble-Pumpin B and Griessen R 1999 *Nature* **399** 439

[3] Huijbregtse J M, Klaassen F C, Szepielow A, Rector J H, Dam B, Griessen R, Kooi B J and de Hosson J T M 2002 *Supercond. Sci. Technol.* **15** 395

[4] Foltyn S R, Civale L, MacManus-Driscoll J L, Jia Q X, Maiorov B, Wang H and Maley M 2007 *Nat. Mater.* **6** 631

[5] Civale L 1997 *Supercond. Sci. Technol.* **10** A11

[6] Wee S H, Goyal A, Martin P M and Heatherly L 2006 *Supercond. Sci. Technol.* **19** 865

[7] Cai C, Holzapfel B, Hanishch J, Fernandez L and Schultz L 2004 *Phys. Rev. B* **69** 104531

[8] Gapud A A, Kumar D, Viswanathan S K, Cantoni C, Varela M, Abiade J, Pennycook S J and Christen D K 2005 *Supercond. Sci. Technol.* **18** 1502

[9] Haugan T, Barnes P N, Wheeler R, Meisenkothen F and Sumption M 2004 *Nature* **430** 867

[10] MacManus Driscoll J L, Foltyn S R, Jia Q X, Wang H, Serquis A, Civale L, Maiorov B, Hawley M E, Maley M P and Peterson D E 2004 *Nat. Mater.* 3 439

[11] Goyal A, Kang S, Leonard K J, Martin P M, Gapud A A, Varela M, Paranthaman M, Ijaduola A O, Specht E D, Thompson J R, Christen D K, Pennycook S J and List F A 2005 *Supercond. Sci. Technol.* **18** 1533

[12] Mele P, Matsumpto K, Ichinose A, Mukaida M, Yoshida Y, Horii S and Kita R

2008 *Supercond. Sci. Technol.* **21** 125017

[13] Varanasi C V, Burke J, Wang H, Lee J H and Barnes P N 2008 *Appl. Phys. Lett.* **93** 092501

[14] Hanisch J, Cai C, Huhne R, Schultz L and Holzapfel B 2005 *Appl. Phys. Lett.* **86** 122508

[15] Feldmann D M, Holesinger, T G, Maiorov B, Foltyn S R, Coulter J Y and Apodaca I 2010 *Supercond. Sci. Technol.* **23** 095004

[16] Wee S H, Goyal A, Zuev Y L, Cantoni C, Selvamanickam V and Specht E D 2010 *Appl. Phys. Exp.* **3** 023101

[17] Wee S H, Goyal A, Specht E D, Cantoni C, Zuev Y L, Selvamanickam V and Cook S 2010 *Phys. Rev. B* **81** 140503

[18] Varanasi C, Barnes P N, Burke J, Carpenter J and Haugan T 2005 *Appl. Phys. Lett.* **87** 262510

[19] Mele P, Matsumpto K, Horide T, Ichinose A, Mukaida M, Yoshida Y and Horii S 2007 *Supercond. Sci. Technol.* **20** 616

[20] Mele P, Matsumpto K, Horide T, Ichinose A, Mukaida M, Yoshida Y and Horii S 2007 *Supercond. Sci. Technol.* **20** 244

[21] Horide T, Matsumoto K, Ichinose A, Mukaida M, Yoshida Y and Horii S 2007 *Supercond. Sci. Technol.* **20** 303

[22] Huhtinen H, Irjala M, Paturi P, Shakhov M A and Laiho R 2010 *J. Appl. Phys.* **107** 053906

[23] Augieri A, Celentano G, Galluzzi V, Mancini A, Rufoloni A, Vannozzi A, Armenio A A, Petisor T, Cioneta L, Rubanov S, Silva E and Pompeo N 2010 *J. Appl. Phys.* **108** 063906

[24] Nelson D R and Vinokur V M 1993 *Phys. Rev. B* **48** 13060

[25] Mele P, Matsumoto K, Horide T, Ichinose A, Mukaida M, Yoshida Y, Horii S and Kita R 2008 *Supercond. Sci. Technol.* **21** 032002

[26] Ercolano G, Harrington S A, Wang H, Tsai C F and MacManus-Driscoll J L 2010 *Supercond. Sci. Technol.* **23** 022003

[27] Figueras J, Puig T, Obradors X, Kwo W K, Paulius L, Crabtree G. W and Deutscher G 2006 *Nat. Phys.* **2** 402

[28] Horide T, Matsumoto K, Mele P, Yoshida Y, Ichinose A, Kita R, Horii S and Mukaida M 2009 *Phys. Rev. B* **79** 092504

Figure captions:

Fig. 1: Schematic diagram of (a) the PLD chamber and (b) used targets for the deposition of YBCO+BSO and YBCO+YBNO nanocomposite films.

Fig. 2: Schematic diagram of the ablation pattern from the YBCO+BSO and YBCO+YBNO surface modified targets when the target rotation speed is varied.

Fig. 3: Cross-sectional TEM image of YBCO+BSO and YBCO+YBNO nanocomposite films deposited using different target rotation speeds. The formation of columnar nanostructures can be clearly seen in these images.

Fig. 4: Variation of T_C (a) and δT_C (b) with target rotation speed for YBCO+BSO and YBCO+YBNO nanocomposite films deposited using different target rotation speeds.

Fig. 5: Variation of J_C and F_p with applied magnetic field at 77 K for YBCO+BSO ((a) and (c)) and YBCO+YBNO ((b) and (d)) nanocomposite films.

Fig. 6: Variation of J_C and F_p with applied magnetic field at 65 K for YBCO+BSO ((a) and (c)) and YBCO+YBNO ((b) and (d)) nanocomposite films.

Fig. 7: Variation of self-field J_C and $F_{pmax.}$ with target rotation speed for YBCO+BSO and YBCO+YBNO nanocomposite films at 77K ((a) and (c)) and 65K ((b) and (d)).

Fig. 8: Variation of J_C with the orientation of applied magnetic field with respect to the *c*-axis for YBCO, YBCO+BSO and YBCO+YBNO films measured at 77 K and 1 T.

Fig. 9: Comparison of irreversibility lines for pure YBCO, YBCO+BSO and YBCO+YBNO nanocomposite films under the condition of *H*//*c*-axis.

Table caption:

Table 1: Comparative analysis of several superconducting parameters for YBCO, YBCO+BSO and YBCO+YBNO films.

List of figures

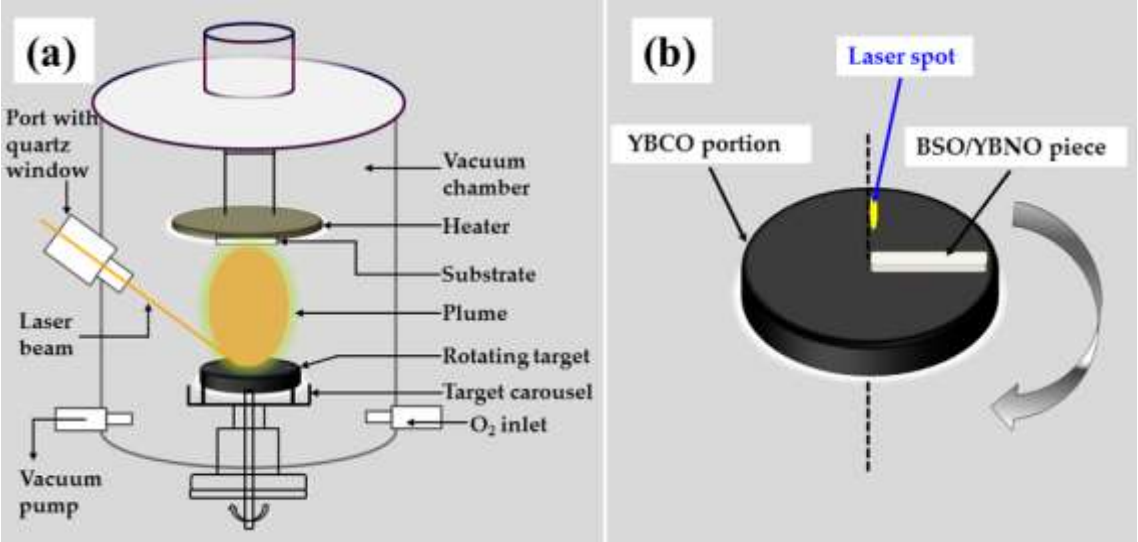

Fig. 1: Schematic diagram of (a) the PLD chamber and (b) used targets for the deposition of YBCO+BSO and YBCO+YBNO nanocomposite films.

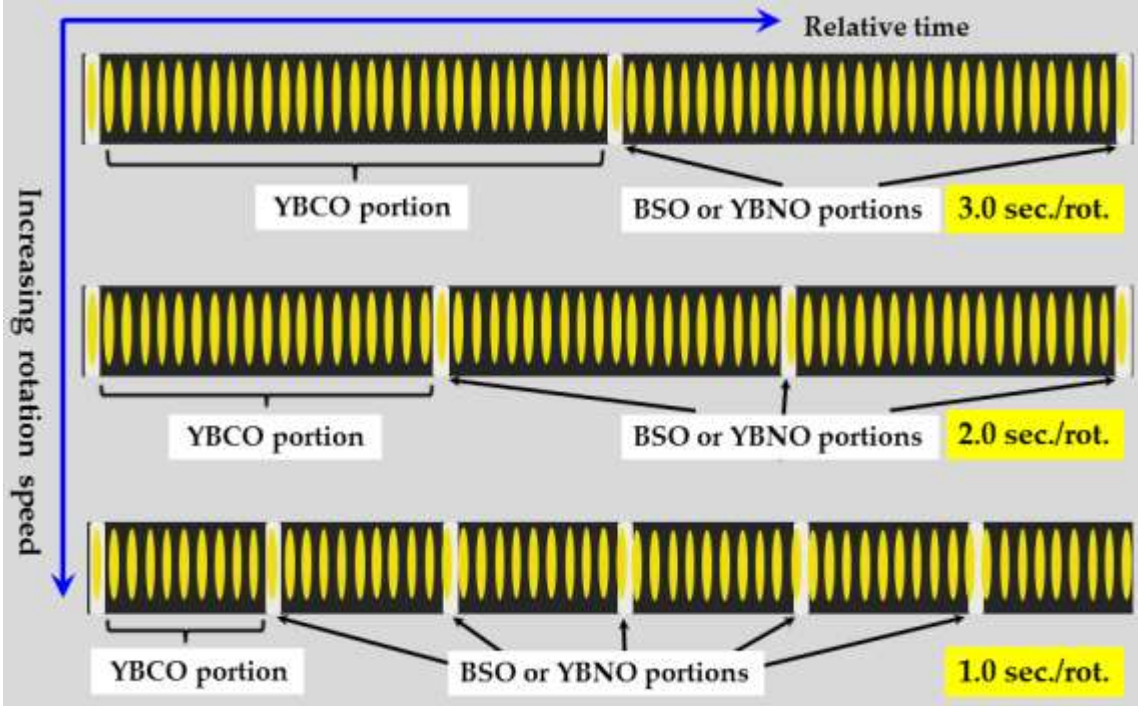

Fig. 2: Schematic diagram of the ablation pattern from the YBCO+BSO and YBCO+YBNO surface modified targets when the target rotation speed is varied.

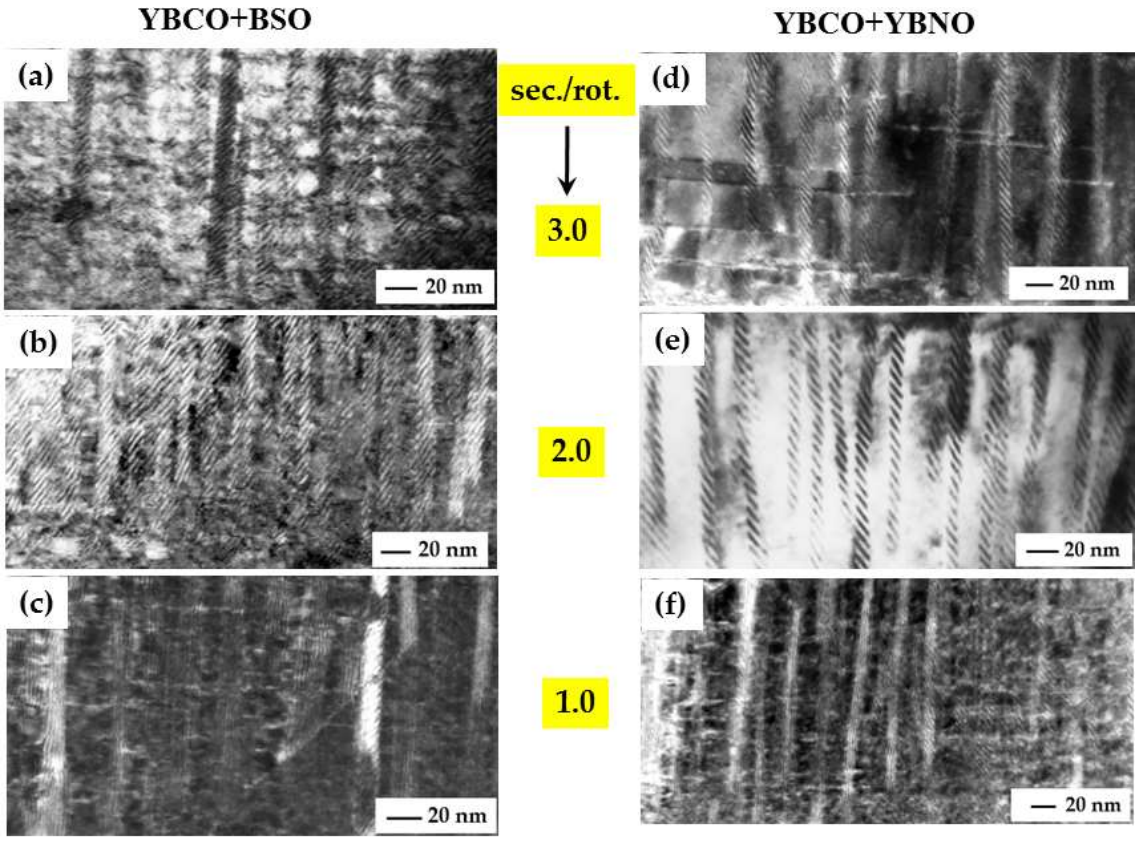

Fig. 3: Cross-sectional TEM image of YBCO+BSO and YBCO+YBNO nanocomposite films deposited using different target rotation speeds. The formation of columnar nanostructures can be clearly seen in these images.

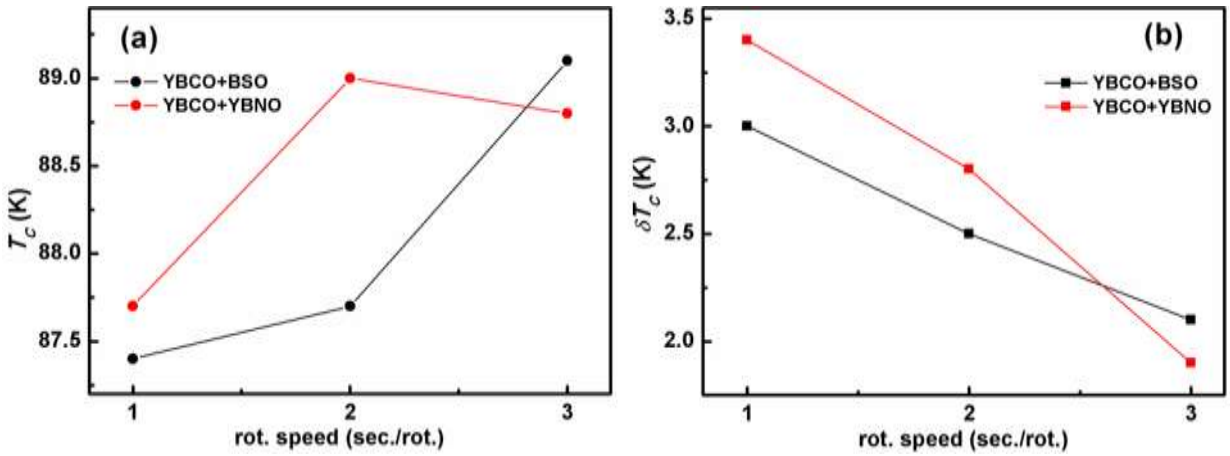

Fig. 4: Variation of T_C (a) and δT_C (b) with target rotation speed for YBCO+BSO and YBCO+YBNO nanocomposite films deposited using different target rotation

speeds.

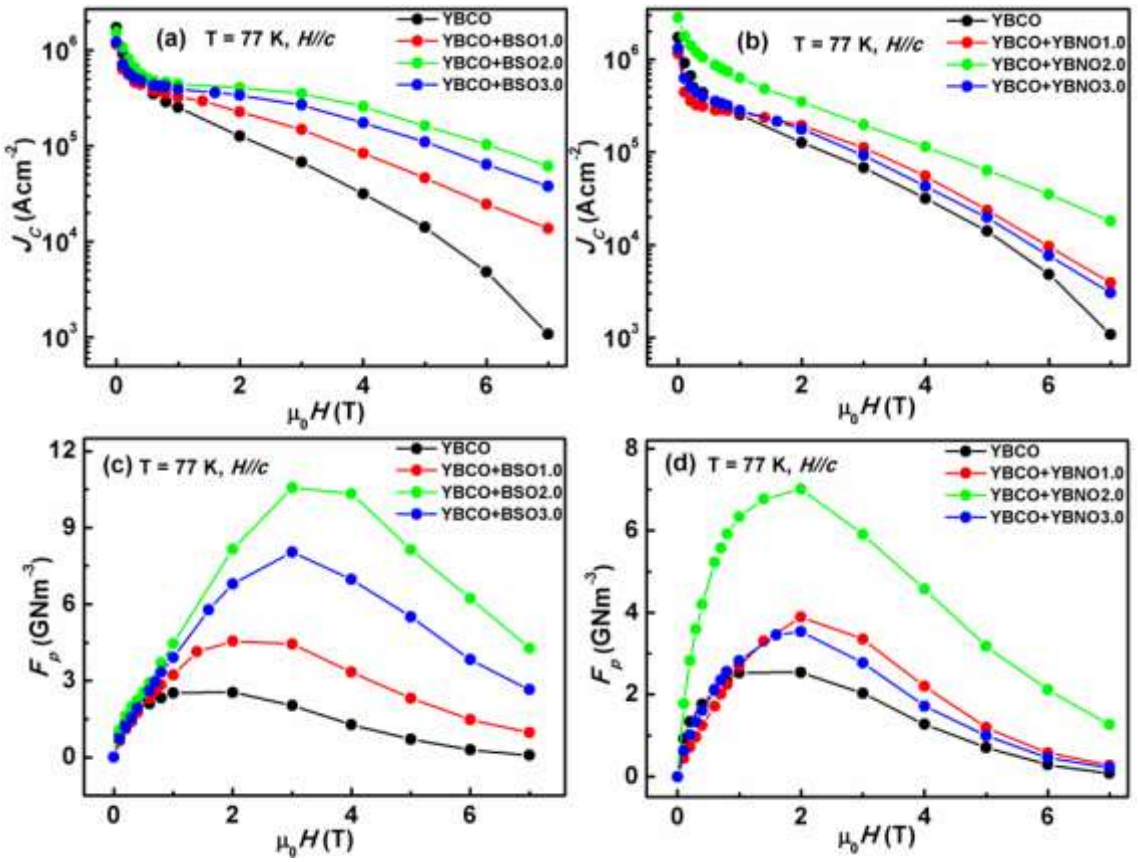

Fig. 5: Variation of J_C and F_p with applied magnetic field at 77 K for YBCO+BSO ((a) and (c)) and YBCO+YBNO ((b) and (d)) nanocomposite films.

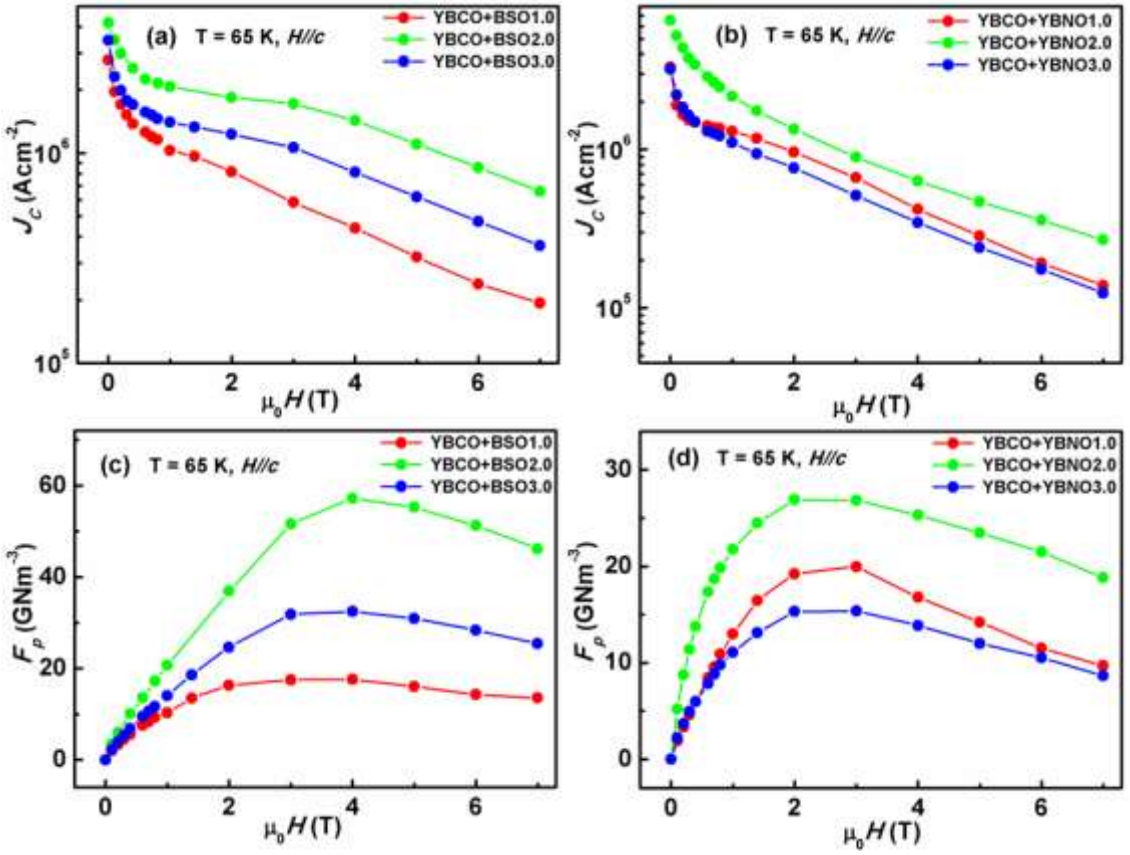

Fig. 6: Variation of J_C and F_p with applied magnetic field at 65 K for YBCO+BSO ((a) and (c)) and YBCO+YBNO ((b) and (d)) nanocomposite films.

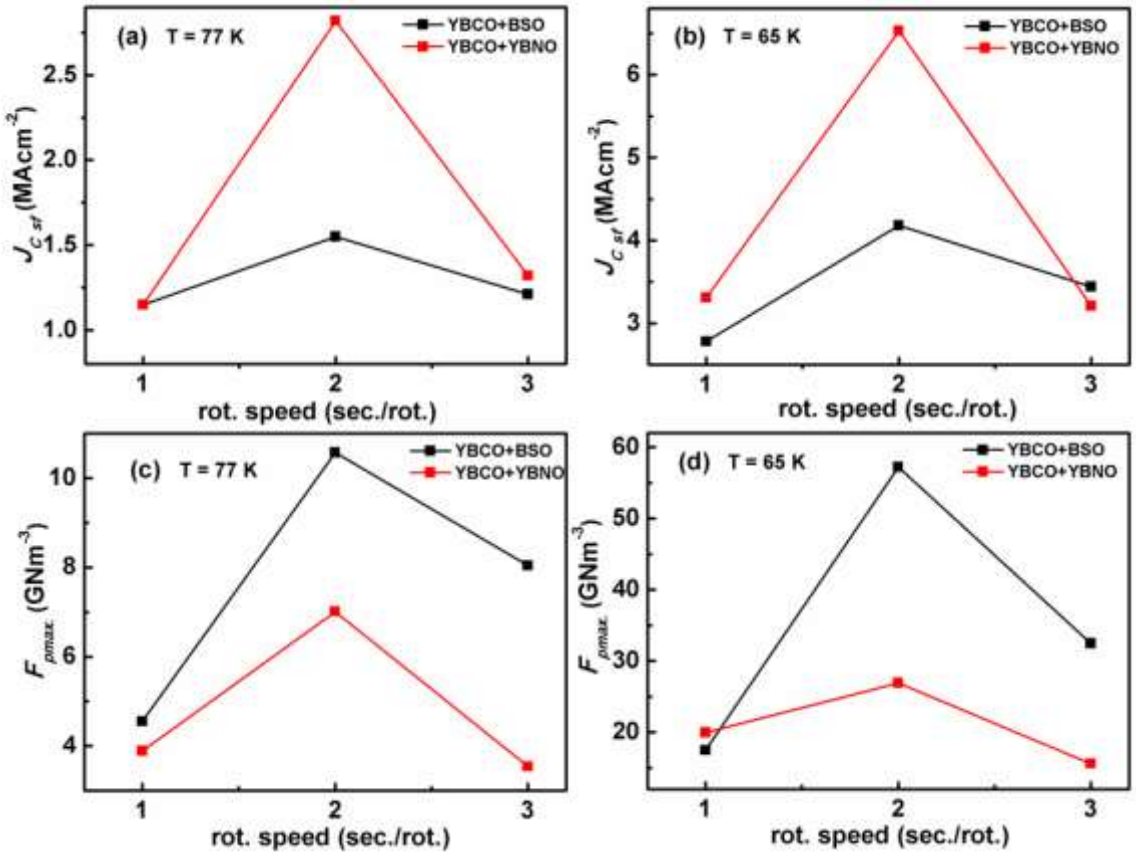

Fig. 7: Variation of self-field J_C and $F_{pmax.}$ with target rotation speed for YBCO+BSO and YBCO+YBNO nanocomposite films at 77K ((a) and (c)) and 65K ((b) and (d)).

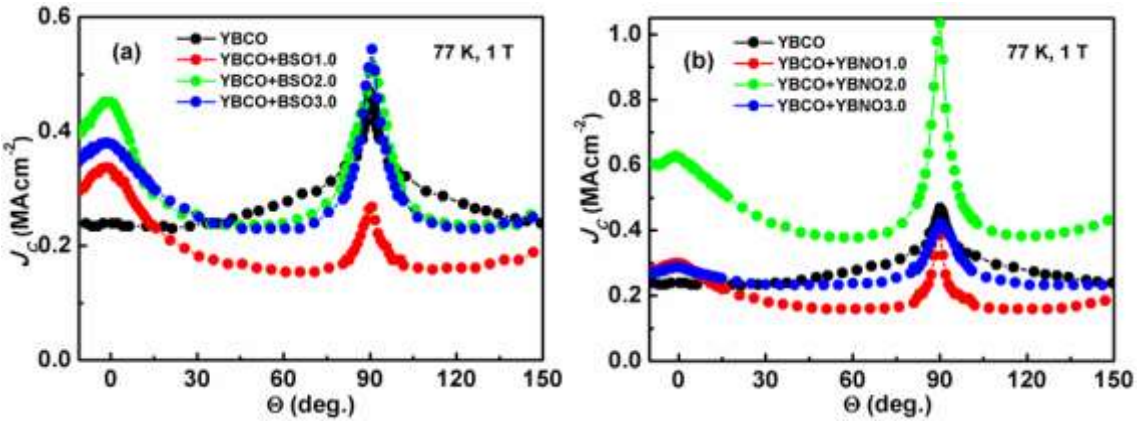

Fig. 8: Variation of J_C with the orientation of applied magnetic field with respect to the *c*-axis for YBCO, YBCO+BSO and YBCO+YBNO films measured at 77 K and 1 T.

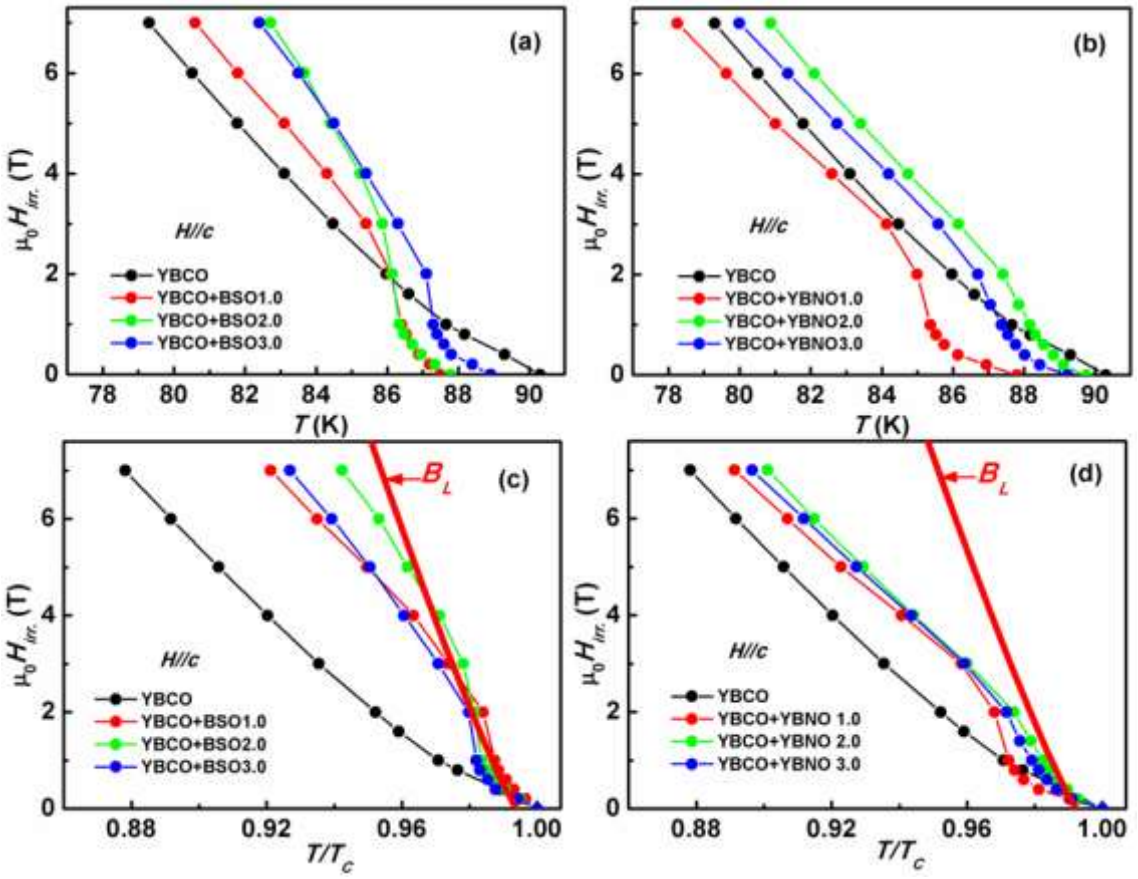

Fig. 9: Comparison of irreversibility lines for pure YBCO, YBCO+BSO and YBCO+YBNO nanocomposite films under the condition of *H//c*-axis.

Table 1: Comparative analysis of several superconducting parameters for YBCO, YBCO+BSO and YBCO+YBNO films

Composition	$T_C(0)$ (K)	δT_C (K)	J_C 0 T, 77 K B // c (MA cm^{-2})	J_C 1 T, 77 K B // c (MA cm^{-2})	$F_{pmax.}$, 77 K B // c (GN m^{-3})	$B_{max.}$ 77 K	J_C 0 T, 65 K B // c (MA cm^{-2})	J_C 3 T, 65 K B // c (MA cm^{-2})	$F_{pmax.}$, 65 K B // c (GN m^{-3})	$B_{max.}$ 65 K	α 77 K	$B_{irr.}$ 77 K
YBCO	89.8	1.2	1.72	0.25	2.54	2					0.57	8.8
YBCO:BSO1.0	87.4	3.0	1.15	0.32	4.55	2	2.78	0.58	17.49	3	0.28	10.0
YBCO:BSO2.0	87.7	2.5	1.55	0.45	10.57	3	4.18	1.72	57.21	4	0.37	13.4
YBCO:BSO3.0	89.1	2.1	1.21	0.39	8.04	3	3.44	1.06	32.47	4	0.27	12.2
YBCO:YBNO1.0	87.7	3.4	1.15	0.28	3.89	2	3.31	0.67	19.98	3	0.24	7.9
YBCO:YBNO2.0	89.0	2.8	2.82	0.63	7.01	2	6.53	0.90	26.92	2	0.44	9.9
YBCO:YBNO3.0	88.8	1.9	1.32	0.27	3.54	2	3.21	0.48	15.60	2	0.36	9.2